Bidirectional Crosstalk and Back-Reflection Free WDM Active Optical Interconnects

Paolo Pintus, *Member, IEEE*, Nicola Andriolli, Fabrizio Di Pasquale, *Member, IEEE*, and John E. Bowers, *Fellow, IEEE*

***Abstract*— In this letter, we present an integrated solution for bidirectional WDM optical interconnection based on semiconductor optical amplifiers and nonreciprocal micro-ring resonators in Si_3N_4/Ce:YIG. The circuit performance has been numerically evaluated, demonstrating a reduction of crosstalk and back-reflection of >20 dB for a 10-channel 100-GHz-spaced WDM bidirectional active optical interconnect. Although a silicon-nitride platform has been considered, the proposed solution can be effective also on a silicon platform, where back-scattering induced by the waveguide roughness is much stronger.**

***Index Terms*— Integrated optics devices, isolators, magneto-optic systems, resonators.**

I. Introduction

NEXT generation data centers and high performance computing systems will be characterized by a very high demand for interconnection bandwidth and tight power consumption constraints [1]. To meet these requirements, integrated optical technologies, already utilized on point-to-point links, will be introduced to perform high-throughput, low-latency, and energy-efficient switching [2]. Optical interconnection networks (as schematically shown in Fig. 1) require multiplexers, de-multiplexers and cascaded switching elements to handle WDM signals from/to the connected racks: they will therefore suffer high losses, especially in large optical switching fabrics.

In this letter, we propose an integrated solution, exploiting hybrid semiconductor optical amplifiers (SOA) [3], to guarantee robust bidirectional transmission of WDM signals through optical interconnection networks [4]. High-gain optical amplifiers are seriously affected by several detrimental effects, such as back-reflections (BR) and cross-gain modulation (XGM). While XGM can be effectively limited by operating the amplifiers in a low saturation regime, large BR cause gain modulation or lasing in the worst case scenario, as well as homowavelength signal crosstalk (XT) related to the amplified signal double back-scattering. To overcome these issues, several solutions have been proposed for interleaved bidirectional optical fiber communication systems [5], [6]. However, no effective solutions have been proposed yet in integrated optics. Taking advantage of the non-reciprocal properties of magneto-optical materials [7], we present an integrated solution based on a single integrated bidirectional optical amplifier (BOA) for WDM bidirectional optical interconnects.

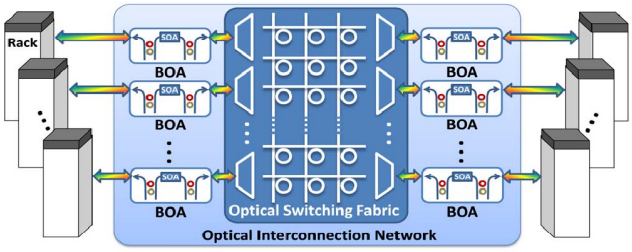

Fig. 1. Bidirectional optical amplifier (BOA) used for bidirectional WDM link.

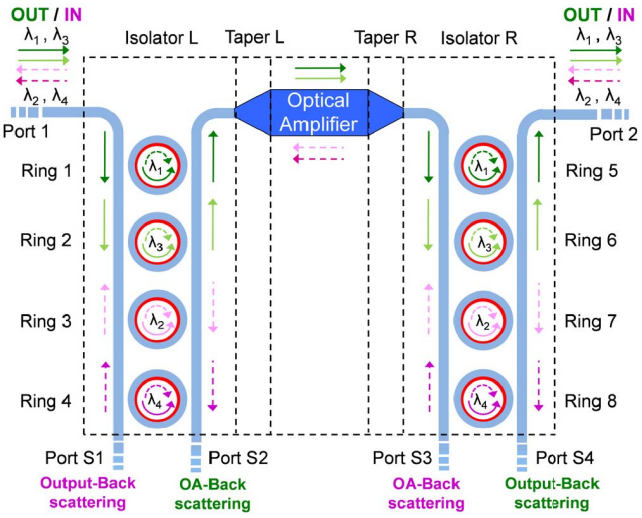

Fig. 2. Bi-directional optical amplifier layout.

II. Proposed Device

The proposed BOA is schematically shown in Fig. 2, where "Isolator L" and "Isolator R" refer to left-hand-side (LHS) and right-hand-side (RHS) wavelength-selective isolators, respectively. Both optical isolators are identical and consist of an array of non-reciprocal ring resonators (four in the picture) which couple two waveguides. In the same figure, "Taper L" and "Taper R" are the waveguide/SOA mode converters on LHS and RHS, respectively [8], [9].

Manuscript received June 22, 2013; revised August 21, 2013; accepted August 22, 2013. Date of publication September 5, 2013; date of current version September 19, 2013.

P. Pintus, N. Andriolli, and F. Di Pasquale are with Scuola Superiore Sant'Anna, Pisa 56124, Italy (e-mail: p.pintus@sssup.it; n.andriolli@sssup.it; f.dipasquale@sssup.it).

J. E. Bowers is with the Department of Electrical and Computer Engineering, University of California, Santa Barbara, CA 93106 USA (e-mail: bowers@ece.ucsb.edu).

Color versions of one or more of the figures in this letter are available online at http://ieeexplore.ieee.org.

Digital Object Identifier 10.1109/LPT.2013.2280153

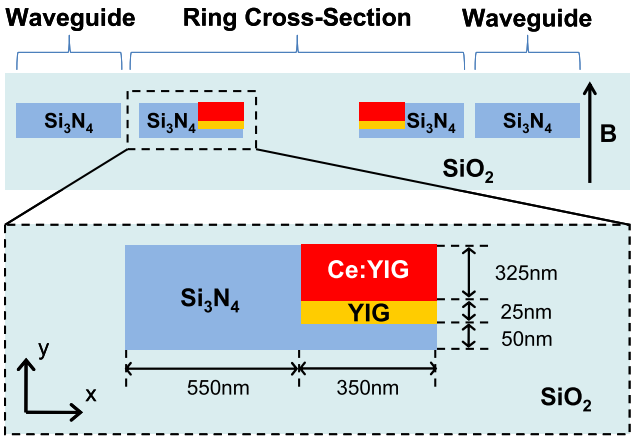

Fig. 3. Cross section of non-reciprocal TE micro-ring resonators.

Using the ultra-low loss silicon nitride platform, non-reciprocal ring resonators can be manufactured by growing a magneto-optical garnet on Si_3N_4 with pulse laser deposition (PLD) technique, as described in [10]. After the fabrication of rings and waveguides, the internal side of the resonators is partially etched, leaving a thin silicon nitride (Si_3N_4) layer (50 nm). On such a base, a thin yttrium iron garnet (YIG) layer (25 nm) can be deposited followed by a rapid thermal annealing at high temperatures to crystallize it. Eventually a Ce:YIG layer (325 nm) is grown with PLD on the YIG seed, providing a suitable ring resonator cross section for TE modes [7]. As experimentally demonstrated, Faraday rotation of such a magneto-optic film is over 4000 deg/cm at $\lambda = 1550$ nm. By applying a vertical magneto-static field (B in Fig. 3), the symmetry of the ring is broken by the non-reciprocal phase shift (NRPS) effect, and the clock-wise (CW) and the counter-clock-wise (CCW) mode propagation constants will be differentiated, resulting in different resonant wavelengths for the two directions. For the sake of clarity, the ring resonator cross section for TE modes is shown in Fig. 3, where the thickness and the width of the layers have been chosen according to [7] in order to maximize the non-reciprocal phase shift effect. For those values, the ring is single mode and a resonance wavelength split of $\Delta\lambda \sim 0.29$ nm (corresponding to ~ 36 GHz) is achieved for the TE mode.

Note that suitable ring resonator cross-sections can also be realized for TM modes [7] and that, depending on the actual transmission modulation format, a polarization diversity scheme can be used to preserve polarization information. However, as we expect that future optical interconnection networks will be based on intensity modulation direct detection (IM-DD), polarization information would not need to be preserved and a single TE polarization scheme could also be effectively used, exploiting a polarization rotator circuit at the BOA input.

In the following analysis we assume to excite TE modes only at the device input. We neglect the ASE contribution, since it is not expected to be the main source of noise in the proposed WDM optical interconnection scheme. On the other hand, the main source of penalty in a bidirectional amplifier scheme is expected to be related to crosstalk induced by scattering and reflections.

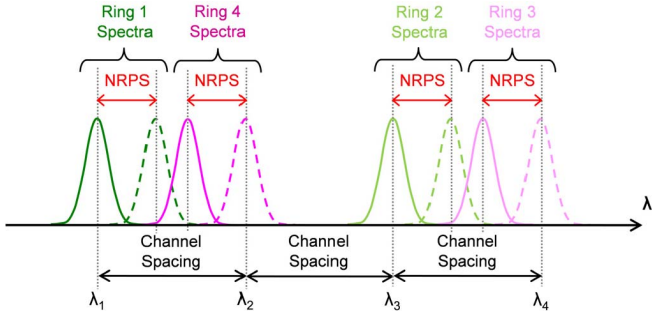

Fig. 4. Isolator spectra. Continuous and dashed lines refer to CCW and CW resonances, respectively.

In order to explain the physical behavior of the proposed integrated BOA, let us consider as an example a four-channel WDM signal with carriers λ_1, λ_2, λ_3, λ_4. The odd channels (λ_1 and λ_3) are injected from Port 1 while the even channels (λ_2 and λ_4) are injected from Port 2 in Fig. 2. Let us design the rings such as λ_1 and λ_3 are the CCW wavelength resonances of the rings 1 and 2 in Isolator L (rings 5 and 6 in Isolator R), respectively. Similarly λ_2 and λ_4 are the CW wavelength resonances of the rings 3 and 4 in Isolator L (rings 7 and 8 for Isolator R), respectively. Moreover, the ring radii are chosen such as their free spectral range (FSR) is larger than the WDM comb. The ring resonator spectra are shown in Fig. 4, where the green lines refer to the rings 1 and 2 (rings 5 and 6), and the magenta lines refer to the rings 3 and 4 (rings 7 and 8).

When λ_1 and λ_3 are injected from Port 1, the two channels propagate separately through rings 1 and 2 toward the optical amplifier. After being amplified, those signals are coupled out to Port 2 through the rings 5 and 6 in the isolator R on the RHS in Fig. 2. Because of the non-reciprocal effect, the BRs from the amplifier are not coupled back to the Port 1 and propagate towards Port S2, being all the rings (from 1 to 4) out of resonance at λ_1 and λ_3. Similarly, the BRs from Port 2 at those two wavelengths propagate back to Port S4 because the rings (5–8) are out of resonance in the CW direction at λ_1 and λ_3. In the same way, we can describe the propagation of the even channels from Port 2 to Port 1. Indeed, it can be easily proved that the back-scatterings from the amplifier and the output port are sent to Port S3 and Port S1, respectively. As a result, also the double BR that cause XT at the output port are significantly reduced. Note that each ring can be independently thermally tuned to align its resonance to the required channel.

III. Mathematical Model

The transmission coefficients of the isolators have been computed using the transfer matrix approach as reported in [7]. Using a silicon nitride platform [11], we assumed a 0.1 dB/cm waveguide propagation loss and 3 dB/cm loss in the rings. To evaluate the performance of the system, we assumed a Gaussian shape for the input modulated signal channels with a 3 dB bandwidth of 10 GHz. A 10-channel 100-GHz-spaced (0.8 nm) WDM interleaved grid has been considered where the odd channels are injected from the LHS, while the even

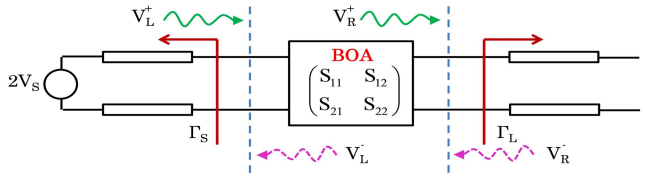

Fig. 5. The transmission line model of the BOA.

channels are sent from the RHS. Each channel is coupled only to a single ring, for this reason the FSR of the ring must be larger than 8 nm (channel spacing × number of channels).

The considered amplifier gain spectrum reported in [12] corresponds to an averaged linear gain of ∼19 dB with a 1.0 mm-long SOA. Note that with an input power per channel of −23 dBm (−16 dBm total input power for 5 WDM channels per direction) the hybrid SOA operates in the low saturation regime, thus effectively limiting XGM effects [13]. This assumption is well justified by the recent demonstration of heterogeneously integrated devices with performance approaching the native InP based devices [14]; the SOA saturated output power in our calculation is 11 dBm. Concerning the tapers, we assumed an insertion loss of 0.5 dB and a BR as small as −55 dB. The transfer matrix of the BOA is computed by multiplying all the building block transfer functions (isolators, tapers and SOA), which can be converted into the scattering matrix

$$\begin{pmatrix} V_L^- \\ V_R^+ \end{pmatrix} = \begin{pmatrix} S_{11} & S_{12} \\ S_{21} & S_{22} \end{pmatrix} \begin{pmatrix} V_L^+ \\ V_R^- \end{pmatrix} \tag{1}$$

The superscripts + and − indicate the waves that propagate from left to right (L→R) and from right to left (R→L), respectively; the subscripts L and R refer for LHS and RHS sections, respectively. In Fig. 5, the proposed device configuration is sketched using the transmission line model, where the equivalent Thevenin circuit is used for the LHS source (V_S) [15].

The BR coefficients from the load and from the source are indicated with Γ_L and Γ_S, respectively. Combining the scattering equations of the BOA with the source and load back-reflected waves, we define the LHS effective BR coefficient S_{11}^{eff} and the left-to-right effective transmission coefficient S_{21}^{eff} as

$$\begin{cases} S_{11}^{\text{eff}} \overset{\text{def}}{=} \dfrac{V_L^-}{V_S} = \dfrac{S_{11} - \Gamma_L (S_{11}S_{22} - S_{12}S_{21})}{1 - S_{11}\Gamma_S - S_{22}\Gamma_L + \Gamma_L\Gamma_S (S_{11}S_{22} - S_{12}S_{21})} \\ S_{21}^{\text{eff}} \overset{\text{def}}{=} \dfrac{V_R^+}{V_S} = \dfrac{S_{21}}{1 - S_{11}\Gamma_S - S_{22}\Gamma_L + \Gamma_L\Gamma_S (S_{11}S_{22} - S_{12}S_{21})} \end{cases} \tag{2}$$

Similarly, we define the RHS effective BR coefficient S_{22}^{eff}, and the right-to-left effective transmission coefficient S_{12}^{eff}. As already mentioned, the output signal might be seriously affected by XT caused by the amplified double BR or, more generally, by multi-path amplified signal (MAS). To estimate the XT between output signal and the MAS we can write the second equation in (2) as

$$V_R^+ = S_{21}^{\text{eff}} V_S = \underbrace{S_{21} V_S}_{\text{amplified}} \text{ signal} + \underbrace{(S_{21}^{\text{eff}} - S_{21}) V_S}_{\text{multi-path amplified signal}} \tag{3}$$

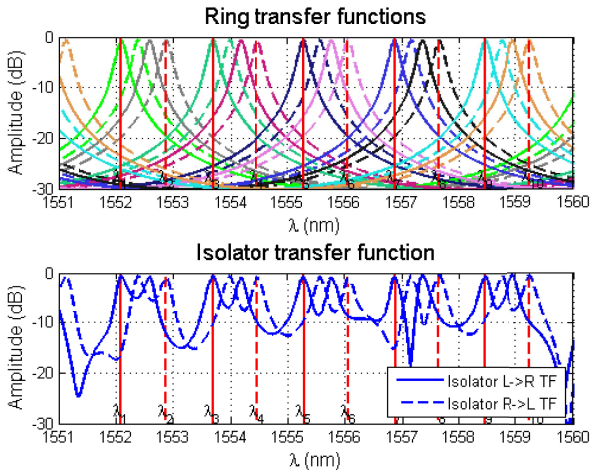

Fig. 6. Transfer function (TF) of ten rings (on the top) and of the isolator (on the bottom). Continuous and dashed lines refer to L→R and R→L propagation, which correspond to CCW and CW resonances, respectively.

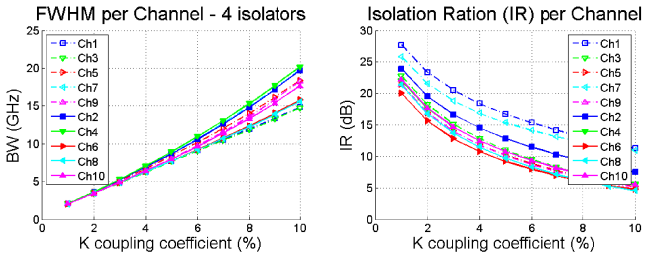

Fig. 7. Full width at half maximum bandwidth (FWHM) of four cascaded isolators and isolation ration (IR) of a single isolator as a function of the ringwaveguide power coupling coefficient K.

The XT on the amplified signal at LHS is then obtained as $XT_L = (S_{21}^{\text{eff}} - S_{21})/S_{21}$. Assuming $\Gamma_L = \Gamma_S = -25$ dB, we have computed the output, the BR and the MAS spectra at the integrated amplifier input and output respectively.

IV. Results

For a 10-channel 100-GHz-spaced WDM interleaved grid, the resulting WDM signal spectrum is 8 nm wide. To avoid that a ring is coupled to more than one channel, the ring radius has been chosen equal to 22 μm, which guarantees a FSR of 8.13 nm. Fig. 6 shows the transfer function of the rings (on the top) and of the isolator (on the bottom), with respect to the two directions, i.e. L→R (CCW) and R→L (CW). The shift between the two spectra for a ring has been maximized according to [7].

To guarantee a 10 GHz wide bandwidth after a cascade of two BOAs (see Fig. 1), we have computed the full width at half maximum bandwidth (FWHM) of four cascaded isolators as a function of the ring-waveguide power coupling coefficient K. As we can see from the Fig. 7, K equal to 6% guarantees a 10 GHz wide bandwidth, allowing for NRZ on-off keyed data transmission at 5 Gb/s per channel. Note that higher rates can be provided by increasing the WDM channel spacing and optimizing the ring parameters. To complete this analysis, Fig. 7 also shows the isolation ratio (IR) as a function of K for a single isolator at the 10 channel wavelengths. As we can see, K equal to 6% provides an IR between 8 and 15 dB. Note

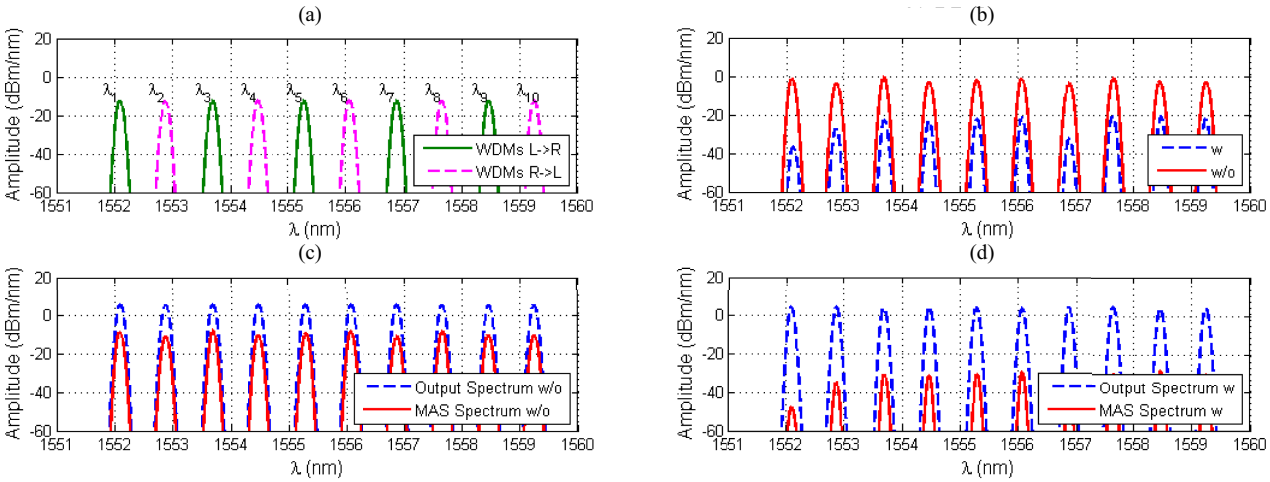

Fig. 8. Input, back-reflection (BR) output, and multi-path amplified (MAS) spectra are shown, which have been computed with (w) and without (w/o) isolators. (a) Input signal spectrum. (b) BR spectrum. (c) XT without isolators. (d) XT with isolators.

that our calculations show that, for the same value of K, an insertion loss lower than 1 dB (not shown in the figure) is achieved for a single isolator.

Finally, we have reported in Fig. 8a the spectra of the 10 channels at the input of the amplifier; the output, the BR and the MAS spectra, calculated with (w) and without (w/o) isolators, are reported in Fig. 8b, 8c and 8d. For the sake of clarity, let us observe that the output spectra are S_{21}Vs for LHS input signal and S_{12}Vs for RHS input signal, respectively; the BR at the two input ports are S_{11}^{eff}Vs for LHS input signal and S_{22}^{eff}Vs for RHS input signal, respectively while the MAS spectra at the output ports are $(S_{21}^{\text{eff}} - S_{21})$Vs for LHS input signal and $(S_{12}^{\text{eff}} - S_{12})$Vs for RHS input signal, respectively.

The output spectra with and without isolators differ by $\sim$2 dB, which corresponds to the insertion loss of the isolators. Vice versa, BR and MAS spectra can be strongly reduced when the proposed devices are used. Indeed, as we can see from Fig. 8b, the BR is reduced by 20 dB for all the considered channels. Similarly, the MAS in Fig. 8c, is decreased by more than 20 dB in the whole band of interest when the isolators are used, as shown in Fig. 8d. Note in addition that without isolators the BR and MAS levels are higher than the injected signal and comparable to the output spectra, inducing SOA gain saturation and making the bidirectional amplifier unusable. As we have shown, such detrimental effects can be effectively reduced by employing the two proposed wavelength selective isolators. Note that the non-uniform spectral shape of the BR and of the MAS at the bottom of Fig. 8 is due to the spectral gain shape of the SOA [12], which is also enhanced by Fabry-Pérot interference induced by the taper BRs.

V. Conclusion

In this letter we have presented a new active interconnect architecture for WDM bi-directional communication. The numerical results have shown the benefit of the BOA in term of XT and BR reduction. Although the link performance has been evaluated using a silicon-nitride platform, the same architecture can be exploited also on a silicon platform, where the back-scattering reflection induced by the waveguide roughness are even stronger.

References

[1] P. Kogge, "Exascale computing study: Technology challenges in achieving exascale systems," DARPA IPTO, USA, Tech. Rep., Sep. 28, 2008.
[2] C. Kachris and I. Tomkos, "A survey on optical interconnects for data centers," *Commun. Surveys Tuts.*, vol. 14, no. 4, pp. 1021–1036, Oct. 2012.
[3] H. Park, *et al.*, "A hybrid AlGaInAs-silicon evanescent preamplifier and photodetector," *Opt. Express*, vol. 15, no. 21, pp. 13539–13546, 2007.
[4] P. Pintus, N. Andriolli, F. Di Pasquale, and J. E. Bowers, "Integrated bidirectional optical amplifier for crosstalk-free WDM communication," in *Proc. IEEE Opt. Interconnects Conf.*, May 2013, pp. 106–107, paper WB2.
[5] K. Tai, *et al.*, "Wavelength-interleaving bidirectional circulators," *IEEE Photon. Technol. Lett.*, vol. 13, no. 4, pp. 320–322, Apr. 2001.
[6] M. S. Lee, I. K. Hwang, and B. Y. Kim, "Bidirectional wavelength-selective optical isolator," *Electron. Lett.*, vol. 37, no. 14, pp. 910–912, 2001.
[7] P. Pintus, F. Di Pasquale, and J. E. Bowers, "Integrated TE and TM optical circulators on ultra-low-loss silicon nitride platform," *Opt. Express*, vol. 21, no. 4, pp. 5041–5052, 2013.
[8] J. F. Bauters, *et al.*, "Silicon on ultra-low-loss waveguide photonic integration platform," *Opt. Express*, vol. 21, no. 1, pp. 544–555, 2013.
[9] G. Kurczveil, P. Pintus, M. J. R. Heck, J. D. Peters, and J. E. Bowers, "Characterization of insertion loss and back reflection in passive hybrid silicon tapers," *IEEE Photon. J.*, vol. 5, no. 2, pp. 6600410-1–6600410-10, Apr. 2013.
[10] M. C. Onbasli, T. Goto, K. Taichi, H. Dong, L. Bi, and C. Ross, "Integration of Magneto-optical cerium-doped YIG on silicon nitride films for nonreciprocal photonic devices," in *Proc. Frontiers Opt.*, pp. 1–3, paper FTu1A.4.
[11] J. F. Bauters, *et al.*, "Planar waveguides with less than 0.1 dB/m propagation loss faBRicated with wafer bonding," *Opt. Express*, vol. 19, no. 24, pp. 24090–24101, 2011.
[12] G. Kurczveil, M. J. R. Heck, J. D. Peters, J. M. Garcia, D. Spencer, and J. E. Bowers, "An integrated hybrid silicon multiwavelength AWG laser," *IEEE J. Sel. Topics Quantum Electron.*, vol. 17, no. 6, pp. 1521–1527, Nov./Dec. 2011.
[13] L. H. Spiekman, *et al.*, "8×10 Gb/s DWDM transmission over 240 km of standard fiber using a cascade of semiconductor optical amplifiers," *IEEE Photon. Technol. Lett.*, vol. 12, no. 8, pp. 1082–1084, Aug. 2000.
[14] B. R. Koch, *et al.*, "Integrated silicon photonic laser sources for telecom and datacom," in *Proc. Opt. Fiber Commun. Conf./Nat. Fiber Opt. Eng. Conf.*, 2013, pp. 1–3, paper PDP5C.8.
[15] D. M. Pozar, *Microwave Engineering*, 3rd ed. Hoboken, NJ, USA: Wiley, 2005.